

## In Situ Fe K-edge X-ray Absorption Spectroscopy of a Nitrosyl Iron(II) Porphyrin Adduct Adsorbed on a High-Area Carbon Electrode in Aqueous Electrolytes

In Tae Bae, Yuriy Tolmachev, Yibo Mo, and Daniel Scherson\*

Department of Chemistry, Case Western Reserve University, Cleveland, Ohio 44106-7078

W. Robert Scheidt and Mary K. Ellison

The Department of Chemistry and Biochemistry, University of Notre Dame, Notre Dame, Indiana 46556

Ming-Chu Cheng, Robert S. Armstrong, and Peter A. Lay

School of Chemistry, University of Sydney, NSW, 2006, Australia

Received December 27, 2000

The first in situ Fe K-edge X-ray absorption spectroscopic (XAS) study is reported on the electronic and structural properties of a nitrosyl iron porphyrin adduct adsorbed on an electrode surface. The specific species was formed, in this case, by exposure of the water-insoluble complex [*meso*-tetrakis(*p*-methoxyphenyl)porphyrinato] iron(II) ([Fe(TMPP)]) adsorbed onto high-area carbon (Black Pearls, ca. 1000–1500 m<sup>2</sup> g<sup>-1</sup>) to aqueous acid solutions containing nitrite. The adsorbed nitrosyl-Fe(TMPP) adduct, denoted as [Fe(NO)(TMPP)](ads), displays remarkable stability over a rather wide potential range. The X-ray absorption near-edge structure (XANES) and the X-ray absorption fine structure (XAFS) are characteristic of an [Fe<sup>II</sup>(TMPP)(NO)(OH<sub>2</sub>)] species, in agreement with assignments proposed for solution-phase nitrosyl iron porphyrin adducts.<sup>1</sup>

The chemistry and biochemistry of molecular and ionic forms of nitrogen oxides continues to be the subject of intense fundamental and technological studies. Interest in this area spans a wide variety of disciplines, ranging from atmospheric sciences and toxicology to electrocatalysis and neurobiology. In particular, nitrogen oxides, derived from the burning of fossil fuels and coal, represent one of the most serious threats to the environment and human welfare.<sup>2,3</sup> Yet, as discovered fairly recently, nitric oxide (NO) is essential for many biological functions,<sup>4,5</sup> including vasodilation and neuronal communication. A better understanding of the electrochemical properties of nitrogen oxides may be expected to contribute greatly to the rational design of effective electrocatalysts for selective reductions, to yield added-value nitrogen compounds from inexpensive and abundant sources, and to the further optimization of highly specific, highly sensitive sensors for in vivo detection of nitric oxide.<sup>6,7</sup>

Of special interest to the present contribution is the work of Meyer and co-workers, who identified the water-soluble complex [*meso*-tetrakis(*p*-sulfonatophenyl) porphyrinato]iron(II) ([Fe(TPPS)]) as an effective electrocatalyst for nitrite reduction in aqueous electrolytes.<sup>1</sup> According to these authors, this redox process proceeds via the formation of a nitrosyl complex intermediate, represented as [Fe<sup>II</sup>(NO<sup>+</sup>)(TPPS)]<sup>3-</sup>, generated by a reaction between [Fe<sup>III</sup>(OH<sub>2</sub>)(TPPS)]<sup>3-</sup> and NO derived from the chemical decomposition of nitrous acid in mildly acidic nitrite solutions.<sup>1</sup> Similar electrocatalytic effects have also been observed in aqueous electrolytes by Su and co-workers for certain Mn and Co porphyrins,<sup>8</sup> and much earlier by Xing et al. for tetrasulfonated cobalt phthalocyanine<sup>9</sup> adsorbed on smooth carbonaceous surfaces. The electrochemical properties of solution-phase species and the identity of their oxidized and/or reduced forms can be characterized by a variety of spectroelectro-chemical methods. However, the extent to which information derived from such studies may be directly relevant to the same, or closely related species adsorbed on electrode surfaces, remains to be established. For example, adsorption may involve chemical bonding, leading to possible modifications in the electronic environment surrounding the redox site. This factor can give rise to shifts in redox potentials and thus to changes in the electrocatalytic activity. In addition, surface immobilization will result in much higher local concentrations than those realizable with species in solution because of solubility limitations, and hence, this will promote more facile multiple electron-transfer reactions. It becomes, therefore, imperative to employ in situ spectroscopic methods with sufficient sensitivity and specificity to elucidate the nature of adsorbed species as a function of the applied potential.

Electrodes were prepared by mixing thoroughly a monolayer dispersion of [Fe<sup>III</sup>(TMPP)Cl] (0.2 mg) in Black Pearls (BP) high-area carbon (Cabot Corp.) (ca. 22% w/w) with a Teflon suspension (T30B, DuPont, 5 mg mL<sup>-1</sup>, 10 μL). The resulting paste was then firmly pressed onto a 1 × 0.5 cm<sup>2</sup> hydrophobic carbon sheet (Eltech Corp.), which served as the current collector. A gold foil and a reversible hydrogen electrode (RHE), placed in separate compartments, were used as counter and reference electrodes, respectively. Measurements were performed in an aqueous NaH<sub>2</sub>PO<sub>4</sub>/H<sub>3</sub>PO<sub>4</sub> buffer (pH 3.1). The nitrosyl complex of [Fe(TMPP)]

\* To whom communication should be addressed.

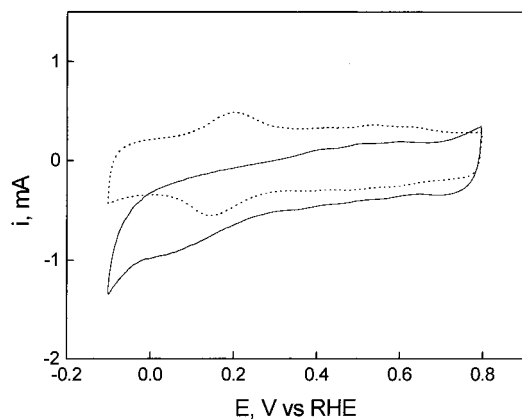
- (1) Barley, M. H.; Takeuchi, K. J.; Meyer, T. *J. Am. Chem. Soc.* **1986**, *108*, 5876–5885.
- (2) Wark, K.; Warner, C. F. *Air-Pollution-Its Origins and Control*; Harper and Row: New York, 1981.
- (3) Yaverbaum, L. H. *Nitrogen Oxides Control and Removal*; Noyes Data Corporation: New Jersey, 1979; Vol 374.
- (4) Lancaster, J. *Nitric Oxide Principles and Actions*; Academic Press: London, New York, 1996.
- (5) Parker, L. *Nitric Oxide Part A: Sources and Detection of NO.; NO Synthase*. Academic Press: London, New York, 1996. Parker, L. *Nitric Oxide Part B: Physiological and Pathological Processes*. Academic Press: London, New York, 1996. Parker, L. *Nitric Oxide Part C: Biological and Anti-Oxidant Activities*. Academic Press: London, New York, 1999.
- (6) Wink, D. A.; Christodoulou, D.; Ho, M.; Krishna, M. C.; Cook, J. A.; Haut, H.; Randolph, J. K.; Sullivan, M.; Coia, G.; Murray, R.; Meyer, T. *Methods: Companion Methods Enzymol.* **1995**, *7*, 71–77.

- (7) Pariente, F.; Maskus, M.; Wu, Q.; Toffanin, A.; Shapleigh, J. P.; Abruna, H. D. *Anal. Chem.* **1996**, *68*, 3128–3134.
- (8) Cheng, S.-H.; Su, Y. O. *Inorg. Chem.* **1994**, *33*, 5847–5854. Yu, C.-H.; Su, Y. O. *J. Electroanal. Chem.* **1994**, *368*, 323–327.
- (9) Xing, X.; Tanaka, A. A.; Fierro, C.; Scherson, D. A. Abstract # 727, 170<sup>th</sup> Electrochemical Society Meeting, Fall 1986.

**Table 1.** Fe(III)-site Dimensions in Fe(TMPP)(NO) Determined by MS XAFS Analyses<sup>a</sup>

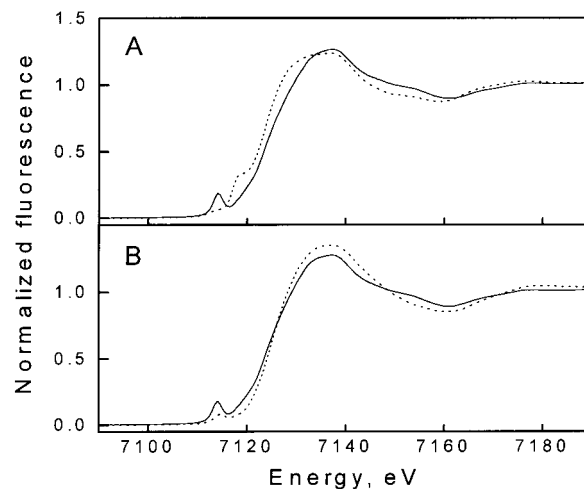
	R (%)	E <sub>0</sub> (eV)	S <sub>0</sub> <sup>2</sup>	Fe–N1 (Å)	Fe–N(NO) (Å)	N–O (Å)	Fe–O (Å) <sup>b</sup>	σ <sub>N1</sub> (Å <sup>2</sup> )	σ <sub>N(NO)</sub> (Å <sup>2</sup> )	σ <sub>O(NO)</sub> (Å <sup>2</sup> )	σ <sub>O</sub> (Å <sup>2</sup> )	Fe–N–O (deg)
[Fe(TMPP)(NO)]	20.05	7125.8	1.05	2.00	1.74	1.10		0.0025	0.0019	0.0056		153.0
[Fe(TMPP)(NO)(O)]	18.57	7127.4	0.85	1.99	1.74	1.10	2.02	0.0024	0.0011	0.0039	0.0031	154.6
[Fe(TPP)(NO)]	14.2	7126.8	0.99	2.01	1.74			0.003	0.005			155

<sup>a</sup> Typical estimated errors were 0.02 Å for the Fe–L bond lengths. <sup>b</sup> Although the typical errors obtained from the analysis were similar for all of the three Fe–L bond lengths, the accuracy of the Fe–O bond length will be less than the others because of its proximity to the four Fe–Np bond lengths; however, the Fe–O bond length is consistent with model complexes.

**Figure 1.** Cyclic voltammograms of [Fe(TMPP)Cl]/BP in phosphate buffer solutions (pH = 3.1) recorded at 5 mV s<sup>-1</sup> in the presence (solid curve) and in the absence of NaNO<sub>2</sub> (dotted curve).

was formed in situ by first cycling the [Fe<sup>III</sup>(TMPP)Cl]/BP electrode between -0.2 and 1.0 V, until features characteristic of the choride-free form of the macrocycle were observed, and then injecting an aliquot of 0.1 M NaNO<sub>2</sub> directly into the cell to a final concentration of ca. 10 mM. In situ Fe K-edge XAS were collected in the fluorescence mode at the Stanford Synchrotron Radiation Laboratory (SSRL, beam line 4-3) using a 13-element Ge detector. Details of the spectroelectrochemical cell, and acquisition and analysis of in situ XANES measurements are described elsewhere.<sup>10</sup> XAFS were analyzed using the XFIT program<sup>11</sup> and models for the NO/porphyrin adducts that were described elsewhere.<sup>12,13</sup>

The steady-state cyclic voltammogram of [Fe(TMPP)]/BP in nitrite-free phosphate buffer, pH 3.1 (Panel A, Figure 1, dotted line), displays a reversible set of redox peaks centered at 0.2 V versus RHE, which are characteristic of the [Fe<sup>III/II</sup>(TMPP)]<sup>+0</sup> couple. Upon addition of nitrite (10 mM) to that solution, these peaks disappeared yielding a featureless trace (solid line). A loss of the Fe(III/II)-based redox couple has also been reported for myoglobin (Mb) incorporated into dimethyldidodecylammonium bromide (ddba) films deposited on pyrolytic graphite electrodes in deaerated NO saturated pH 7.4 buffer aqueous solutions.<sup>14</sup> The negative currents observed over the wide potential range in Figure 1 appear to be unrelated to the presence of the adsorbed porphyrin, as the same behavior was found for the same type of macrocyclic-free BP carbon electrodes. Similar negative currents were observed by Meyer and co-workers<sup>1</sup> in nitrite-containing electrolytes in the presence of the water-soluble [Fe(TPPS)]. The in situ Fe K-edge XANES collected before addition of nitrite at 0.0 V (dotted line,

**Figure 2.** In situ Fe K-edge XANES of [Fe(TMPP)]/BP in phosphate buffer (pH = 3.1) aqueous solutions at 0.0 V (A) and 0.5 V (B) before (dotted curves) and after (solid curves) injecting NaNO<sub>2</sub> (final concentration 10 mM).

Panel A, Figure 2) is characteristic of a ferrous porphyrin. The spectrum collected at 0.5 V (dotted line, Panel B) is characteristic of a ferric porphyrin. Both spectra are in agreement with those reported earlier by us.<sup>15</sup> Addition of nitrite while the electrode was polarized at either one of these potentials resulted in marked changes in the corresponding in situ XANES (solid lines in panels A and B, Figure 2). However, no discernible differences between the spectra obtained at these two potentials were apparent, i.e., one and the same species appear to be formed after addition of nitrite, regardless of whether the original adsorbed species is in the reduced (0.0 V) or oxidized state (0.5 V). Redox reactions involving NO and nitrite have been proposed for the case of the water-soluble [Fe(TPPS)], referred to above, to account for the formation of the species denoted as [Fe<sup>II</sup>(NO\*)(TPSS)]<sup>4-</sup> and for Fe<sup>III</sup>-heme,<sup>16</sup> for which the local environments surrounding the Fe center are analogous to those in FeTMPP. Particularly prominent in the XANES of the NO-free adsorbed species is the pre-edge feature at 7115 eV, for which the intensity is significantly increased in the presence of nitrite; this is similar to the changes observed in the formation of NO adducts of heme proteins.<sup>13,17</sup>

Analysis of the in situ EXAFS based on the average of four spectral acquisitions at 0.5 V was carried out assuming both a five- and a six-coordinate iron center and a linear and bent NO axial ligand. Based on the results collected in Table 1, the adsorbed NO adduct is best represented as a six-coordinate ferrous nitrosyl porphyrin complex, with water as the most probable ligand in the position trans to the nitrosyl group. Attempts to model the site with a structure involving a five- or six-coordinate

(10) Bae, I. T.; Scherson, D. A. *J. Phys. Chem.* **1996**, *100*, 19215–19217.

(11) Ellis, P. J.; Freeman, H. C. *J. Synchrotron Rad.* **1995**, *2*, 190–195. This program incorporates FEFF 6.01 for MS (Rehr, J. J.; Albers, R. C.; Zabinsky, S. I. *Phys. Rev. Lett.* **1992**, *69*, 3397–3400).

(12) Rich, A. M.; Armstrong, R. S.; Ellis, P. J.; Lay, P. A. *J. Am. Chem. Soc.* **1998**, *120*, 10827–10836.

(13) Rich, A. M.; Armstrong, R. S.; Ellis, P. J.; Freeman, H. C.; Lay, P. A. *Inorg. Chem.* **1998**, *37*, 5743–5753.

(14) Bayachou, M.; Lin, R.; Cho, W.; Farmer, P. J. *J. Am. Chem. Soc.* **1998**, *120*, 9888–9893.

(15) Kim, S.; Bae, I. T.; Sandifer, M.; Ross, P. N.; Woicik, J.; Antonio, M. R.; Scherson, D. A. *J. Am. Chem. Soc.* **1991**, *113*, 9063–9066.

(16) Hoshino, M.; Maeda, M.; Konishi, R.; Seki, H.; Ford, P. C. *J. Am. Chem. Soc.* **1996**, *118*, 5702–5707.

(17) Rich, A. M.; Ellis, P. J.; Tennant, L.; Wright, P. E.; Armstrong, R. S.; Lay, P. A. *Biochemistry* **1999**, *38*, 16491–16499.

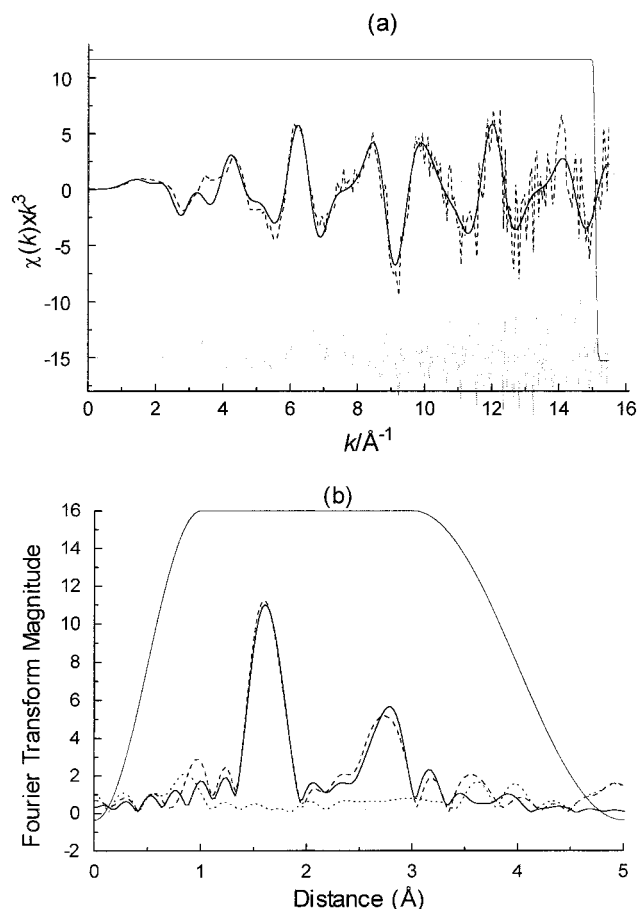


**Figure 3.** (a) XAFS and (b) Fourier transform amplitude of XAFS of the  $[\text{Fe}^{\text{II}}(\text{TMPP})(\text{NO})(\text{OH}_2)]$  adduct observed in situ (—), calculated from refined model (---), residual (···), window used in Fourier filter (—).

linear NO, as for a ferric species, reverted to structures with bent Fe–N–O moieties, supporting the view that the metal center is indeed ferrous in character. In agreement with this assignment is the XANES region, for which the intensity of the pre-edge peak is somewhat smaller than that observed for genuine  $[\text{Fe}^{\text{II}}(\text{TPP})(\text{NO})]$  in crystalline form measured at room temperature. The best multiple-scattering (MS) fit ( $R = 18.6\%$ , Figure 3)<sup>18</sup> to the XAFS data resulted in Fe–N<sub>p</sub>, Fe–N<sub>NO</sub>, and Fe–OH<sub>2</sub> bond lengths of 1.99, 1.74, and 2.02 Å, respectively, and an Fe–N–O bond angle of 155°, these are typical of such  $\text{Fe}^{\text{II}}\text{NO}$  adducts.<sup>12,17,19</sup> It may

(18) The fit was achieved without considering the ortho carbons of the phenyl substituents, but this does not influence the bond lengths and angles, only the  $R$  value.<sup>12</sup> Other information on the refinement is contained in the Supporting Information.

be noted that for the  $\text{Fe}^{\text{II}}\text{NO}^+$  adduct, the Fe–N<sub>NO</sub> bond length and Fe–N–O bond angle would be expected to be  $\sim 1.64$  Å and  $\sim 175^\circ$ , respectively.<sup>12,17,19</sup> This is the first in situ structural characterization of an adsorbed NO–Fe porphyrin adduct in electrochemical environments.

Attempts to oxidize or reduce the adsorbed adduct by polarizing the electrode at potentials more positive than 0.9 V, or more negative than  $-0.1$  V, respectively, yielded in situ XANES that were indistinguishable from those obtained for the formally Fe(II) and Fe(III) forms of the macrocycle never exposed to nitrite. It may be concluded on this basis, that at this low pH, the reduced and oxidized forms of adsorbed  $[\text{Fe}^{\text{II}}(\text{TMPP})(\text{NO})(\text{OH}_2)]$ , if produced, are too short-lived and/or in very low concentrations to be detected by the current XAS technique. In fact, clearly defined redox waves for the reduction of NO–Mb incorporated in ddab films to generate the corresponding nitrosyl adduct could only be discerned at very high scan rates at neutral pH. The wide range of potentials over which  $[\text{Fe}^{\text{II}}(\text{TMPP})(\text{NO})(\text{OH}_2)]$  is stable is consistent with the results of Meyer et al.,<sup>1</sup> who provided evidence that the oxidation and reduction of this specific adduct are separated by about 1 V. The fact that no redox waves attributed to the nitrosyl-free water-soluble FeTPPS were observed by these authors in nitrite containing solutions at about the same pH suggests that the macrocycle undergoes adsorption on the smooth carbon surface, forming a stable NO adduct of the type found in this work. Implications of these results to the Fe–porphyrin mediated electrocatalytic reduction of NO in aqueous electrolytes are currently under study and will be reported in due course.

**Acknowledgment.** This work was carried out at the Stanford Synchrotron Radiation Laboratory, which is supported by the U.S. Department of Energy, Division of Material Sciences and Division of Chemical Sciences. Funding for this work was provided by the National Science Foundation (D.A.S.) and the National Institutes of Health (W.R.S., NIH GM-38401). Additional support was provided by an Australian Research Council Grant (R.S.A. and P.A.L.), and the Access to Major Facilities Program funded by the Department of Industry, Science, and Resources, and managed by the Australian Nuclear Science and Technology Organization.

**Supporting Information Available:** The starting model for  $[\text{Fe}^{\text{II}}(\text{TMPP})(\text{NO})(\text{OH}_2)]$ , tables of the constraint and restraint parameters of the  $[\text{Fe}^{\text{II}}(\text{TMPP})(\text{NO})(\text{OH}_2)]$ , and the final refined atomic positional coordinates for the  $[\text{Fe}^{\text{II}}(\text{TMPP})(\text{NO})(\text{OH}_2)]$ . This material is available free of charge via the Internet at <http://pubs.acs.org>.

IC001460W

(19) Scheidt, W. R.; Ellison, M. K. *Acc. Chem. Res.* **1999**, *32*, 350–359.